# The Damage Tolerance of a Sandwich Panel Containing a Cracked Honeycomb Core

**I. Quintana Alonso**

**N. A. Fleck**[1]
e-mail: naf1@cam.ac.uk

Department of Engineering,
Cambridge University,
Trumpington Street,
Cambridge CB2 1PZ, UK

*The tensile fracture strength of a sandwich panel, with a center-cracked core made from an elastic-brittle diamond-celled honeycomb, is explored by analytical models and finite element simulations. The crack is on the midplane of the core and loading is normal to the faces of the sandwich panel. Both the analytical models and finite element simulations indicate that linear elastic fracture mechanics applies when a K-field exists on a scale larger than the cell size. However, there is a regime of geometries for which no K-field exists; in this regime, the stress concentration at the crack tip is negligible and the net strength of the cracked specimen is comparable to the unnotched strength. A fracture map is developed for the sandwich panel with axes given by the sandwich geometry. The effect of a statistical variation in the cell-wall strength is explored using Weibull theory, and the consequences of a stochastic strength upon the fracture map are outlined.*
[DOI: 10.1115/1.2912995]

*Keywords: finite element analysis, fracture, toughness, elastic behaviour, lattice materials*

## 1 Introduction

Ceramic honeycombs are used in catalytic converters and diesel particulate filters for automobiles, in filters of continuous casting plant, in plates for gas burners, and in medical prosthetic implants. Glass honeycombs have been used as lightweight supports for space mirrors as, for example, in the Hubble telescope. In most of these applications, the ceramic lattices are chosen for their multifunctional properties, such as high thermal shock resistance, high chemical stability, and high stiffness. They are loaded in a sandwich panel configuration with stiff and strong face sheets. The flaw sensitivity of the tensile strength of these honeycombs is of concern and is the motivation for the present study: We shall explore the tensile fracture strength of a sandwich panel, with a center-cracked core made from an elastic-brittle diamond-celled honeycomb. The crack is on the midplane, with loading normal to the face of the sandwich panel, see Fig. 1. The strength is determined both by finite element simulations and by simple analytical models. It will be shown that the tensile strength is dictated by the Mode I fracture toughness of the honeycomb for a limited regime of sandwich panel geometries. Accordingly, we begin by reviewing the fracture toughness of brittle honeycombs.

**1.1 Fracture Toughness of Brittle Honeycombs.** The fracture toughness of brittle hexagonal honeycombs has been modeled by relating the crack tip elastic fields of an equivalent continuum to the stress state within the lattice [1,2]. It was assumed that the macroscopic fracture toughness is set by local tensile failure when the maximum stress in any strut of the lattice attains the fracture strength $\sigma_f$ of the cell-wall material. It is shown that the fracture toughness of the hexagonal honeycomb scales linearly with $\sigma_f$, quadratically with relative density and with the square root of cell size (as demanded by dimensional analysis).

Numerical and analytical predictions for the fracture toughness of several honeycomb topologies are now available. Fleck and Qiu [3] have determined the fracture behavior of isotropic lattices of deterministic fracture strength: hexagonal, triangular, and Kagome. Orthotropic lattices with square cells have also been examined [4]. An analytical model of the fracture toughness of the diamond-celled honeycomb shown in Fig. 2 has been developed and validated by finite element calculations [5]. The diamond-celled honeycomb is remarkably tough: Its Mode I fracture toughness scales as

$$K_{IC} = \beta \sigma_f \bar{t} \sqrt{\ell} \tag{1}$$

where $\bar{t}$ is the ratio of cell-wall thickness $t$ to cell size $\ell$, and the numerical constant is $\beta = 0.44$ [4]. Limited experimental studies of the fracture toughness of honeycombs have been found in the literature. Measurements on notched three point bend specimens of cordierite honeycombs have been carried out by Huang and Gibson [6]. Their data suggest that Eq. (1) gives an adequate description of the fracture toughness of the diamond-celled honeycomb.

Microstructural imperfections, such as wavy struts and displaced joints, are expected to have a knockdown effect on the fracture properties of elastic-brittle honeycombs. The sensitivity of fracture toughness to imperfections in the form of displaced joints has been explored by Romijn and Fleck [4]. They found that the nodal connectivity of the lattice dictates the response. A connectivity of four struts per joint, as in the diamond-celled lattice, is the transition case: The behavior of these structures can be bending-dominated or stretching-dominated depending on the

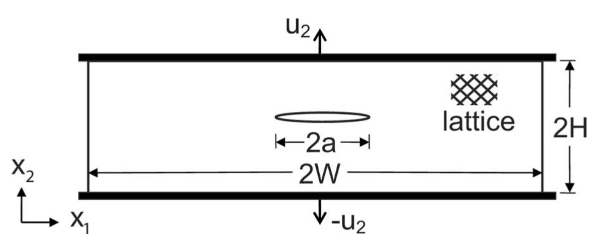


**Fig. 1 Center-cracked sandwich plate made from a diamond-celled honeycomb and subjected to uniaxial tension**

[1]Corresponding author.

Contributed by the Applied Mechanics Division of ASME for publication in the JOURNAL OF APPLIED MECHANICS. Manuscript received July 30, 2007; final manuscript received October 23, 2007; published online July 21, 2009. Review conducted by Robert M. McMeeking.

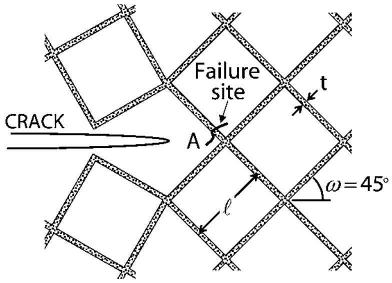


**Fig. 2 Crack morphology**

level of imperfection. Consequently, the fracture toughness of the diamond-celled topology is imperfection sensitive.

Brittle solids exhibit a scatter of failure strengths: Variable flaw sizes and a random orientation within the brittle cell walls lead to variations in the tensile strength of the solid material $\sigma_f$. Huang and Gibson [6] and later Huang and Chou [7] have included statistical effects in the fracture toughness of hexagonal and square honeycombs by assuming that the strength of the cell walls follows a Weibull distribution. They concluded that the fracture toughness $K_{IC}$ increases with cell size if the Weibull modulus $m$ is greater than 4, is insensitive to cell size if $m$ equals 4, and it decreases with cell size if $m$ is less than 4. We shall reassess this result for the diamond-celled honeycomb.

**1.2 Statement of the Problem.** In the present study, we investigate the tensile fracture response of a center-cracked sandwich panel made from a diamond-celled honeycomb (Fig. 1). This is a common test geometry and is representative of practical applications. The sandwich panel is of width $2W$ and height $2H$, and contains a crack of length $2a$. Fixed grip load conditions are applied by prescribing remote displacements, as shown in Fig. 1.

The diamond-celled lattice, sketched in Fig. 2, is characterized by its cell size $\ell$, wall thickness $t$, and core angle $\omega$. However, only orthogonal honeycombs of $\omega=45$ deg are considered in this study. The cell-wall material is linear elastic to fracture. It has Young's modulus $E_s$, Poisson's ratio $\nu_s$, and a deterministic tensile fracture strength $\sigma_f$. Later in our study, we shall modify this by considering a Weibull distribution of strength. The relative density of the diamond-celled honeycomb is defined by the density of the lattice divided by that of the of the cell-wall material, and is related to $\bar{t}\equiv t/\ell$ by

$$\bar{\rho}=\bar{t}(2-\bar{t}) \tag{2}$$

Classical beam theory suffices to analyze the stress state within the sandwich core in the absence of a crack. Straightforward analysis reveals that the sandwich panel has an out-of-plane unnotched tensile strength $\sigma_u$, which scales with the tensile fracture strength of the solid material $\sigma_f$ and with $\bar{t}$ according to

$$\sigma_u=\frac{\bar{t}}{1+3\bar{t}}\sigma_f \tag{3}$$

This expression takes into account both bending and stretching of the cell walls. Upon neglecting the bending contribution, it reduces to

$$\sigma_u=\bar{t}\sigma_f \tag{4}$$

The approximation (4) is acceptable at low relative densities: At $\bar{t}=0.05$, it leads to an error of 15% in Eq. (3). Henceforth, we shall assume that the unnotched strength is given by Eq. (4).

Now introduce a macroscopic crack into the honeycomb. We write $\sigma^\infty$ as the remote gross stress required to initiate crack growth under uniaxial loading. Then $\sigma^\infty/\sigma_f$ depends on the four nondimensional groups $\bar{t}$, $a/\ell$, $H/\ell$, and $H/W$. In the current study, we shall limit attention to practical sandwich geometries for which $H/W$ is small.

**1.3 Scope of the Study.** The structure of this paper is as follows. First, simple analytical models are used to obtain the deterministic fracture strength of the center-cracked panels. These predictions are used to construct a fracture map with axes given by the sandwich beam geometry. The map is validated by selected finite element (FE) simulations. The statistics of brittle fracture are then considered, and the effect of a Weibull distribution of strength on the regimes of dominance of the fracture map is explored.

## 2 Analytic Description

Consider the center-cracked sandwich panel shown in Fig. 1. The failure strength for any given geometry is determined from a series of simple analytical models. We shall show that the effect of geometry on strength is adequately captured by the two nondimensional groups $\ell/a$ and $\ell/(\bar{t}H)$. These groups are used to define the axes of a failure mechanism map, and each analytical model of failure has a *regime* of dominance on the map.

We argue that there exists a Regime I of specimen geometries for which the stresses are uniform throughout the lattice. The stress concentration at the crack tip is negligible and the net strength of the cracked panel equals the unnotched strength: The panel is damage tolerant. However, there exist other geometries for which a $K$-field develops around the crack tip, on a scale larger than the cell size. We call this Regime II if the crack is long compared to the height of the sandwich panel, and Regime III if it is short. A detailed analysis for each regime is now given.

**2.1 Regime I.** A schematic representation of the stress state within the sandwich core for Regime I is shown in Fig. 3(*a*). Elastic shear regions partition zones of uniform stress state within the sandwich panel: equibiaxial stress, uniaxial stress, and zero stress, see Fig. 3(*a*).

A simple physical model can be developed for the macroscopic strength [8]. It is assumed that only bars that connect one face sheet to the other carry load. Bars that end on the crack faces or on the side edges of the sandwich panel are unloaded. The remaining bars connect both face sheets and are subjected to an axial stress on the bar cross section of

$$\sigma_a=\frac{u_2}{2H}E_s \tag{5}$$

The number $n$ of load carrying bars is given by

$$n=\frac{4(W-H-a)}{\ell\sqrt{2}} \tag{6}$$

Equilibrium in the vertical $x_2$-direction of Fig. 3(*a*) gives the relation between the macroscopic gross stress $\sigma^\infty$ and the local tensile stress in the bars $\sigma_a$ as

$$\sigma^\infty=n\frac{t\sqrt{2}}{4W}\sigma_a \tag{7}$$

Failure occurs when the axial stress in the bars, $\sigma_a$, attains the tensile strength of the solid material, $\sigma_f$. The gross-section strength of the sandwich panel follows as

$$\sigma^\infty=\left(1-\frac{H}{W}-\frac{a}{W}\right)\bar{t}\sigma_f \tag{8}$$

The net-section strength is defined by $\sigma_n=\sigma^\infty/(1-a/W)$ and in nondimensional form it reads

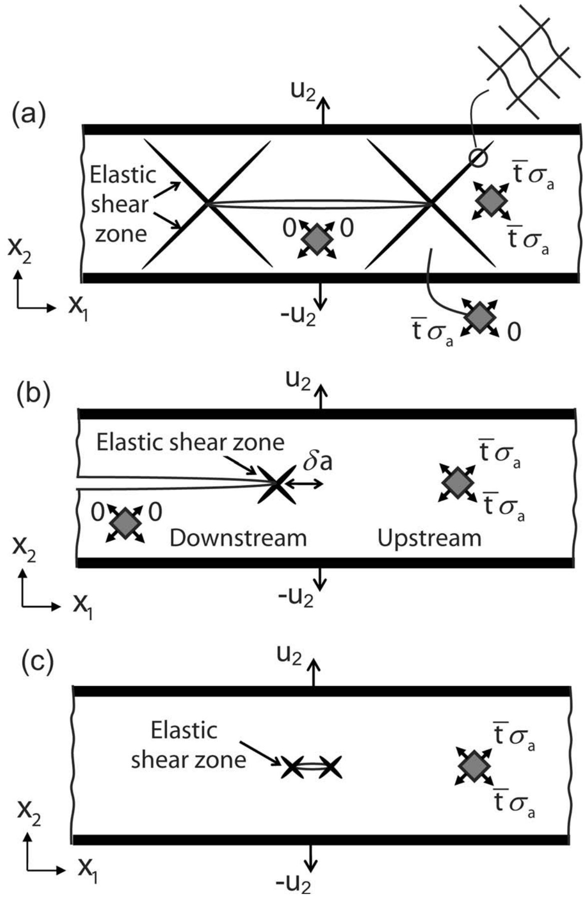


**Fig. 3** (***a***) **Regime I: uniform stress with practically no stress concentration at the crack tip. (*b*) Regime II: *K*-field exists. Strength is independent of crack length. (*c*) Regime III: *K*-field exists. Strength scales with crack length as $a^{-1/2}$. In all three regimes, the effective stress far ahead of the crack tip is equibiaxial, and of magnitude $\bar{t}\sigma_a$ upon neglecting the contribution from beam bending.**

$$\bar{\sigma} \equiv \frac{\sigma_n}{\sigma_u} = \frac{\sigma^\infty}{\left(1 - \frac{a}{W}\right)\sigma_u} \tag{9}$$

Now limit attention to the case $H/W \ll 1$. Substitution of Eq. (8) into Eq. (9) gives $\bar{\sigma}=1$ since $\sigma_u=\bar{t}\sigma_f$ according to expression (4). We emphasize that the nondimensional parameter $\bar{\sigma}$ compares the net-section strength of the cracked sandwich panel to the unnotched strength. It is therefore a measure of the damage tolerance of the sandwich panel.

**2.2 Regime II.** Assume that the crack is sufficiently long compared to the height $2H$ of the sandwich panel that the core behaves as an orthotropic elastic strip with a semi-infinite crack, see Fig. 3(*b*). Upstream of the crack tip, a biaxial state of stress prevails while downstream the core is unloaded. In the intermediate zone, a crack tip *K*-field exists on a length scale larger than that of the cell size. The Mode I stress intensity factor $K_I$ at the crack tip is given by the steady state solution as follows.

First, calculate the energy release rate $G_I$ by advancing the crack tip a virtual increment $\delta a$. The energy released $G_I\delta a$ equals the difference in stored elastic energy within a strip of width $\delta a$ and height $2H$ upstream and downstream of the crack tip. Treat the lattice as an effective medium, subjected to a uniform stress state far ahead of the crack tip and far behind the crack tip. Material elements downstream of the crack tip are unloaded. Upstream, material elements are subjected to the macroscopic strain state $\varepsilon_{11}=\varepsilon_{12}=0$ and $\varepsilon_{22}=u_2/H$. The macroscopic stress component $\sigma_{22}$ is [4]

$$\sigma_{22} = \frac{1}{2}E_s(\bar{t}+\bar{t}^3)\varepsilon_{22} \tag{10}$$

with $\sigma_{12}=0$. Consequently, an energy balance reads

$$G_I\delta a = \frac{1}{2}\sigma_{22}\varepsilon_{22}2H\delta a = \frac{2H\sigma_{22}^2}{E_s(\bar{t}+\bar{t}^3)}\delta a \tag{11}$$

It remains to determine the stress intensity factor $K_I$ in terms of $G_I$.

The energy release rate $G_I$ and the stress intensity factor $K_I$ in an orthotropic material in plane stress are related through the expression

$$G_I = C_I K_I^2 \tag{12}$$

where the elastic coefficient $C_I$ is a function of the elastic moduli, see, for example, Tada et al. [9]. For the orthotropic honeycomb under consideration, $C_I$ is given by

$$C_I = \frac{\sqrt{\bar{t}^2+1}}{\sqrt{2}}\frac{1}{\bar{t}^2 E_s} \tag{13}$$

The stress intensity factor $K_I$ follows as

$$K_I = \frac{2^{3/4}\bar{t}\sigma_{22}\sqrt{H}}{(\bar{t}+\bar{t}^3)^{1/2}(\bar{t}^2+1)^{1/4}} \tag{14}$$

We modify this expression to account for the case of a finite crack. Since $\sigma_{22}$ is the net-section stress, the remote gross stress $\sigma^\infty$ reads

$$\sigma^\infty = (1 - a/W)\sigma_{22}, \tag{15}$$

Also assume that $\bar{t}$ is much less than unity. Then Eqs. (14) and (15) simplify to

$$K_I = F_I\sigma^\infty\sqrt{H} \tag{16}$$

where the calibration function $F_I$ is

$$F_I = \frac{2^{3/4}\sqrt{\bar{t}}}{(1 - a/W)} \tag{17}$$

Recall that Mode I fracture toughness $K_{IC}$ of the diamond-celled lattice has already been given by Eq. (1) in terms of a single numerical constant $\beta=0.44$, as calibrated by FE simulations [4]. Failure occurs when $K_I=K_{IC}$. Consequently, the gross-section strength of the sandwich panel is

$$\sigma^\infty = \frac{K_{IC}}{F_I\sqrt{H}} = 2^{-3/4}\beta\sqrt{\bar{t}}\left(\frac{\ell}{H}\right)^{1/2}\left(1 - \frac{a}{W}\right)\sigma_f \tag{18}$$

and the nondimensional net-section strength reads

$$\bar{\sigma} \equiv \frac{\sigma^\infty}{\left(1 - \frac{a}{W}\right)\sigma_u} = 2^{-3/4}\beta\left(\frac{\ell}{H\bar{t}}\right)^{1/2} \tag{19}$$

We mention in passing that the calibration factor $F_I$ derived here is in excellent agreement with that obtained by Georgiadis and Papadopoulos [10] using Fourier transforms and the Wiener–Hopf technique. Additional FE simulations have been performed for a cracked strip made from an orthotropic continuum. They confirm the accuracy of Eq. (19) for finite $a/W$, and are omitted here for the sake of brevity.

**2.3 Regime III.** Regime III is schematically depicted in Fig. 3(*c*). Now, the crack is much smaller than the height and width of the sandwich panel. The *K*-calibration for an orthotropic panel containing a short central crack of length $2a$ is approximately

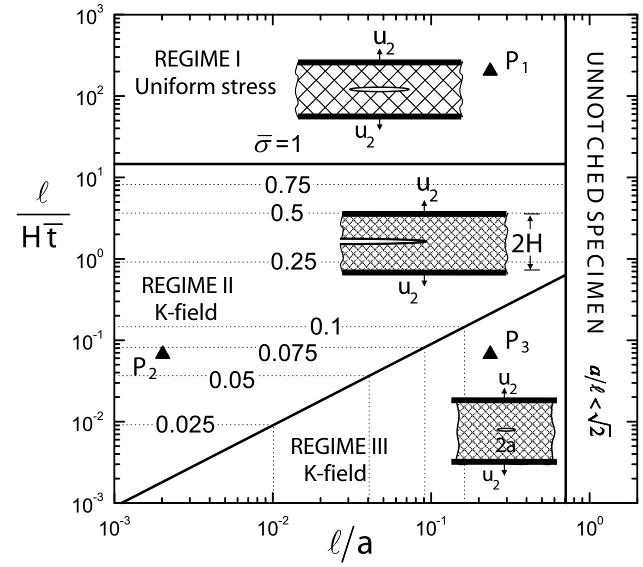


**Fig. 4 Fracture map for a panel containing a center crack and subjected to prescribed displacements. The sample geometries $P_1$, $P_2$, and $P_3$ are explored in detail in Sec. 3 to illustrate the response within each regime.**

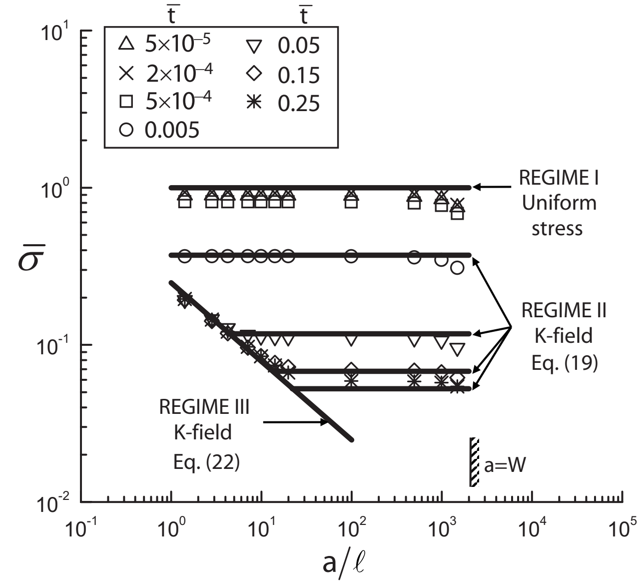


**Fig. 5 Normalized net strength as a function of crack size. The width of the sandwich panel is much larger than its height ($W/H=20$), and its height is much larger than the cell size ($H/\ell=70\sqrt{2}$). The solid lines denote analytic predictions.**

$$K_I = \frac{\sigma^\infty \sqrt{\pi a}}{\left(1-\dfrac{a}{W}\right)} \tag{20}$$

A more precise calibration can be found in the literature [11]. However, the approximate relation (20) is adequate for our purposes and it leads to a major simplification of subsequent algebra.

Failure occurs when the stress intensity factor $K_I$ reaches the critical value, $K_{IC}$. The gross-section strength of the sandwich panel is given by

$$\sigma^\infty = \frac{\left(1-\dfrac{a}{W}\right)K_{IC}}{\sqrt{\pi a}} = \frac{\beta}{\sqrt{\pi}}\bar{t}\left(\frac{\ell}{a}\right)^{1/2}\left(1-\frac{a}{W}\right)\sigma_f \tag{21}$$

and the normalized net-section strength is

$$\bar{\sigma} \equiv \frac{\sigma^\infty}{\left(1-\dfrac{a}{W}\right)\sigma_u} = \frac{\beta}{\sqrt{\pi}}\left(\frac{\ell}{a}\right)^{1/2} \tag{22}$$

**2.4 Construction of the Fracture Map.** The above three analytical models can be used to construct a fracture map, with suitably chosen axes in terms of the sandwich geometry. The nondimensional net-section strength $\bar{\sigma}$ equals unity in Regime I, depends on $\ell/\bar{t}H$ in Regime II, and depends on $\ell/a$ in Regime III. Consequently, we construct a fracture map with axes $(\ell/a, \ell/\bar{t}H)$, as shown in Fig. 4. The boundaries between regimes are obtained by equating the expressions for the strength within each regime. The boundary between Regimes I and II is given by $\ell/\bar{t}H=14.6$ upon taking $\bar{\sigma}=1$ in Eq. (19). Likewise, the boundary between Regimes II and III is obtained by equating $\bar{\sigma}$ from Eq. (19) with $\bar{\sigma}$ from Eq. (22), to give $\ell/\bar{t}H=0.9\ell/a$. A physical constraint on the minimum crack length is also imposed on the map: The minimum crack length in the lattice is $a/\ell=\sqrt{2}$. It is straightforward to add contours of nondimensional strength $\bar{\sigma}$ to the map, upon making use of $\bar{\sigma}=1$ in Regime I, and relations (19) and (22) in Regimes II and III, respectively. We emphasize that the fracture map is universal for all relative densities and for all geometries of sandwich panel, provided $W/H$ is sufficiently large. It remains to perform a series of FE simulations to validate the map.

## 3 Numerical Calculations

Selected FE simulations have been carried out to determine the gross-section fracture strength $\sigma^\infty$ of centrally cracked sandwich panels made from an elastic-brittle, diamond-celled honeycomb. It is assumed that the honeycomb fails when the maximum tensile principal stress anywhere in the lattice attains a critical value $\sigma_f$.

The linear elastic calculations were performed using the commercial FE code ABAQUS (version 6.5-3). Each strut in the lattice was modeled as a two-noded Euler–Bernoulli beam element (type $B23$ in ABAQUS notation): This element uses cubic interpolation functions and allows for both stretching and bending deformations but neglects shear deformation.

The symmetries of the geometry and loading were such that a FE mesh was generated for one-quarter of the sandwich panel. The crack in the lattice was defined by splitting the joints along the cracking plane while keeping intact the struts on each face of the crack (Fig. 2). The face sheets were not explicitly modeled in the FE simulations. Rather, all lattice joints attached to the face sheets were subjected to the same prescribed vertical displacement, with zero transverse displacement and zero rotation.

The FE mesh of the sandwich core comprised 1400 cells in the $x_1$ direction by 70 cells in the $x_2$ direction. Throughout this numerical study, two aspect ratios were held constant: $H/\ell=70\sqrt{2}$ and $H/W=1/20$. We investigated the sensitivity of the fracture strength of the sandwich panel to crack length $a/\ell$ and to relative density as parametrized by $\bar{t}\equiv t/\ell$.

**3.1 Verification of the Regimes of Behavior.** A series of FE calculations has been performed for selected values of $\bar{t}$ in the range $5\times10^{-5}$ to 0.25 and $a/\ell$ between $\sqrt{2}$ and $1050\sqrt{2}$. The results are given in Fig. 5 in the form of a plot of $\bar{\sigma}$ versus $a/\ell$, together with the analytic prediction $\bar{\sigma}=1$ for all $\bar{t}$ in Regime I, the prediction (19) for selected values of $\bar{t}$ in Regime II, and the prediction (22) for all in $\bar{t}$ Regime III. Good agreement between the analytical formulas and numerical predictions is noted for all

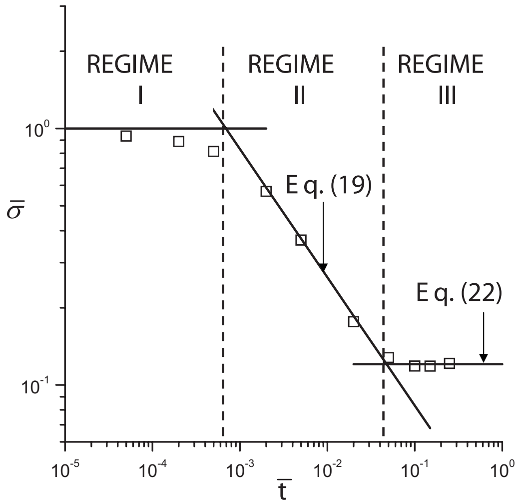


**Fig. 6 Net strength as a function of relative density for a sandwich panel made from a lattice, which contains a central crack of length $a/\ell=3\sqrt{2}$. The panel has aspect ratios $W/H=20$ and $H/\ell=70\sqrt{2}$.**

three regimes. For $\bar{t}$ below a transition value of $\beta^2\ell/2\sqrt{2}H=6.9\times10^{-4}$, the response lies within Regime I: The FE simulations confirm that $\bar{\sigma}\approx1$. For $\bar{t}$ above this transition value, the strength of the sandwich panel is toughness controlled and $\bar{\sigma}$ is below the unnotched value. In Regime II, the strength of the panel is independent of crack length and scales with relative density according to $\bar{\sigma}\propto(\bar{t}H/\ell)^{-1/2}$, recall Eq. (19). In Regime III, the nondimensional strength of the panel is independent of relative density and scales with crack length as $\bar{\sigma}\propto(a/\ell)^{-1/2}$.

Additional insight is obtained by plotting in Fig. 6 the normalized net-section strength $\bar{\sigma}$ as a function of $\bar{t}$; this is done by cross plotting the seven data points of Fig. 5 at fixed $a/\ell=3\sqrt{2}$. Three additional simulations were run and added to Fig. 6 in order to present a more complete comparison between FE results and analytical estimates. At small $\bar{t}$, the response lies within Regime I: No stress concentration exists and the unnotched strength is maintained, $\bar{\sigma}=1$. With increasing $\bar{t}$, the response switches to Regime II and $\bar{\sigma}$ scales as $\bar{t}^{-1/2}$ in accordance with Eq. (19). At large $\bar{t}$, Regime III exists such that $\bar{\sigma}$ is insensitive to $\bar{t}$, as stated in Eq. (22). It is remarkable that the simple estimates of Sec. 2, based on linear elastic fracture mechanics for a continuum, capture the response in Regimes II and III despite the fact that the lattices of Fig. 6 contain only a few broken cells.

**3.2 Normal Traction Directly Ahead of the Crack Tip.** Consider the forces in the joints of the lattice directly ahead of the crack tip. These forces are used to construct a traction distribution on the crack plane directly ahead of the crack tip, in order to make comparisons with the stress state in a cracked continuum. This traction distribution has been obtained for the geometries $P_1$, $P_2$, and $P_3$, as defined in Fig. 4. These geometries are taken to be representative of the response for each of the three regimes.

(i) The traction distribution for geometry $P_1$ (representative of Regime I) is uniform at $\sigma_{22}\approx\sigma^\infty$, see Fig. 7(*a*). This implies that no *K*-field exists.

(ii) The traction $\sigma_{22}(r)$ for geometry $P_2$ of Regime II is compared to the asymptotic crack tip field $\sigma_{22}=K_I/\sqrt{2\pi r}$ in Fig. 7(*a*), where *r* is the distance ahead of the crack tip. Note that Eq. (16) is used for $K_I$. It is clear that the traction in the discrete lattice is consistent with the *K*-field of a continuum.

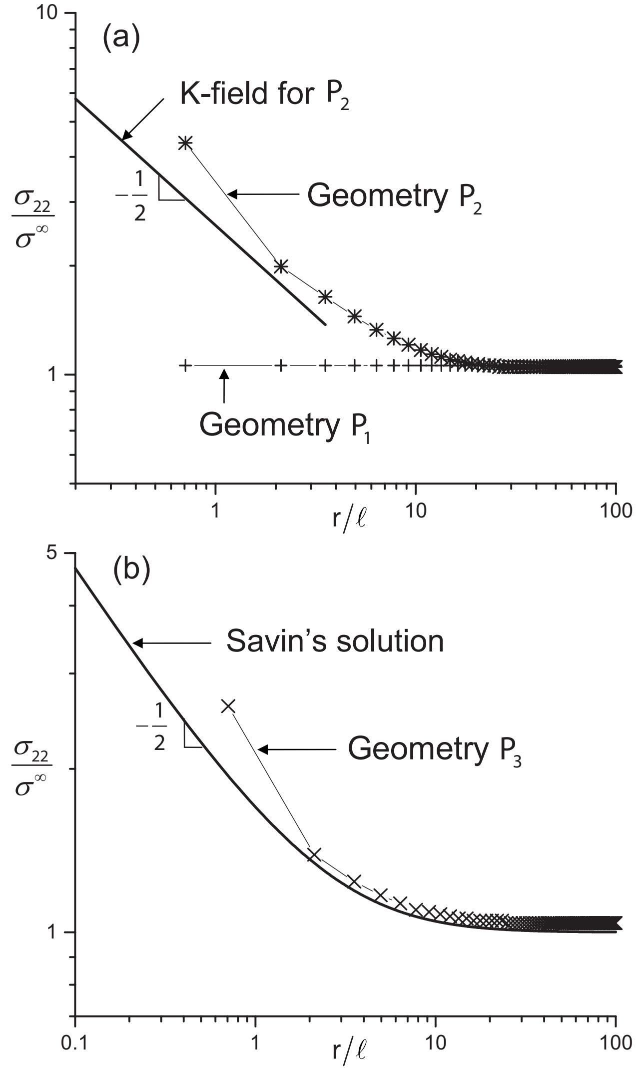


**Fig. 7 Normal tractions directly ahead of the crack tip. The geometries are specified by $P_1$: $\bar{t}=5\times10^{-5}$, $a/\ell=3\sqrt{2}$; $P_2$: $\bar{t}=0.15$, $a/\ell=350\sqrt{2}$, and $P_3$: $\bar{t}=0.15$, $a/\ell=3\sqrt{2}$.**

(iii) Finally, consider geometry $P_3$ of Regime III. The traction within the discrete lattice is plotted in Fig. 7(*b*) along with the Savin [12] solution for an infinite orthotropic panel containing a center crack. It is clear that the traction ahead of the crack tip in the lattice is adequately represented by the continuum solution. The agreement is remarkably close given the fact that the crack in the lattice is short, $a/\ell=3\sqrt{2}$.

The comparisons made in Fig. 7 support the applicability of linear elastic fracture mechanics in Regimes II and III: $K_{IC}$ serves as a useful fracture parameter to describe the local conditions near the crack tip of the lattice.

## 4 Statistics of Brittle Failure

Brittle solids, such as engineering ceramics, contain a random distribution of flaws of stochastic length. Consequently, the solid cell walls of a brittle honeycomb exhibit a statistical distribution of tensile fracture strength $\sigma_f$. Weibull statistics are commonly used to model this scatter in strength: the survival probability $P_s$ of a brittle solid of volume $V$ subjected to a maximum principal tensile stress $\sigma_1$ is given by

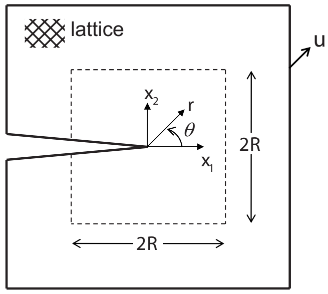


**Fig. 8 FE model used to assess the fracture toughness of the lattice**

$$P_s(\sigma_1) = \exp\left[-\int_V \left(\frac{\sigma_1}{\sigma_0}\right)^m \frac{dV}{V_0}\right] \tag{23}$$

where $m$ is the Weibull modulus and $\sigma_0$ is a reference fracture strength for a reference volume $V_0$. The magnitude of the Weibull modulus is a measure of the variability in strength: The lower the value of $m$, the greater the variability in strength.

We proceed to include the statistical component of cell-wall strength in our analysis of the cracked sandwich panel. Strength-controlled failure (Regime I) and toughness-controlled failure (Regimes II and III) are treated in turn.

**4.1 Strength-Controlled Regime I.** In Regime I, the deterministic net-section strength of the cracked panel is adequately predicted by the unnotched strength $\sigma_u = \bar{t}\sigma_f$. It is straightforward to modify this analysis for a statistical distribution of strength. Assume that the cell walls are uniaxially loaded. Then, the maximum principal tensile stress $\sigma_1$ can be written in terms of the remote applied net-section stress $\sigma_n$ as $\sigma_1 = \sigma_n/\bar{t}$. The Weibull distribution (23) now takes the form

$$P_s(\sigma_n) = \exp\left[-\left(\frac{\sigma_n}{\bar{t}\sigma_0}\right)^m \frac{V}{V_0}\right] \tag{24}$$

The average net-section strength $(\sigma_n)_{\mathrm{mean}}$ immediately follows as

$$(\sigma_n)_{\mathrm{mean}} = \int_0^\infty P_s(\sigma_n)d\sigma_n = \sigma_0\bar{t}\left(\frac{V_0}{V}\right)^{1/m}\Gamma\left(\frac{m+1}{m}\right) \tag{25}$$

where $\Gamma(1+1/m)$ is the gamma function and $V = 4H(W-a)\bar{\rho}$ is the total volume of cell-wall material per unit depth.

**4.2 Statistics of Fracture Toughness.** So far, we have used a deterministic value of fracture toughness; however, statistical variations in the strength of the solid cell walls lead to variations in the fracture toughness of the lattice. We proceed to use Weibull theory to predict the variability in fracture toughness in terms of $m$, $\sigma_0$, and $V_0$.

*4.2.1 Weibull Analysis for a Crack Tip Field.* Consider the problem of a diamond-celled lattice containing a long crack, as sketched in Fig. 8. The polar coordinates $(r,\theta)$ are centered on the crack tip and are defined in the usual manner, see Fig. 8. We subject the outer boundary of the lattice to the displacement field **u** associated with the macroscopic crack tip $K$-field for an orthotropic elastic solid [13].

Write the maximum principal tensile stress $\sigma_1$ within the cell walls of the lattice in the form

$$\sigma_1 = \frac{K_I}{\bar{t}\sqrt{\ell}}g(r/\ell,\theta,\bar{t}) \tag{26}$$

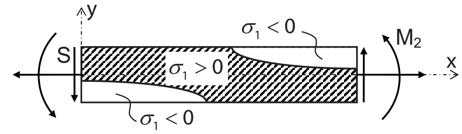


**Fig. 9 Maximum principal stress distribution for a typical strut in the lattice**

where $K_I$ is Mode I stress intensity factor and the function $g$ gives the dependence on position within the lattice and on the bar stubbiness $\bar{t}$.

According to Weibull theory, the probability of survival of the lattice subjected to a stress intensity $K_I$ is found by substituting Eq. (26) into Eq. (23):

$$\begin{aligned} P_s(K_I) &= \exp\left[-\int_V \left(\frac{K_I g}{\sigma_0\bar{t}\sqrt{\ell}}\right)^m \frac{dV}{V_0}\right] \\ &= \exp\left[-\left(\frac{K_I}{\sigma_0\bar{t}\sqrt{\ell}}\right)^m \int_V g^m \frac{dV}{V_0}\right] \end{aligned} \tag{27}$$

The average fracture toughness of the lattice follows as

$$(K_{IC})_{\mathrm{mean}} = \int_0^\infty P_s(K_I)dK_I = \bar{K}\sigma_0\bar{t}\sqrt{\ell} \tag{28}$$

where

$$\bar{K} \equiv \frac{(K_{IC})_{\mathrm{mean}}}{\sigma_0\bar{t}\sqrt{\ell}} = \Gamma\left(\frac{m+1}{m}\right)\left[\int_V g^m \frac{dV}{V_0}\right]^{-1/m} \tag{29}$$

*4.2.2 Finite Element Simulations.* We shall now evaluate $\bar{K}$ from FE simulations. A square mesh of the diamond-celled lattice was created using ABAQUS (version 6.5-3). Each strut of the lattice was modeled as an Euler–Bernoulli beam element. The square mesh was of side 600 unit cells and contained a traction-free edge crack along the negative $x_1$-axis (Fig. 8). Loading was applied by imposing the displacement field corresponding to the $K$-field on the boundary of the mesh [13]. A mesh convergence study based on the maximum local tensile stress in the lattice revealed that the mesh suffices for the present investigation.

$\bar{K}$ is calculated as follows. The maximum principal tensile stress $\sigma_1$ within the cell walls of the lattice is determined from the FE simulations. These stresses are used to obtain the function $g$ as defined in Eq. (26). Note that only the maximum principal tensile stress $\sigma_1$ enters the calculation. Figure 9 shows a typical strut in the lattice with the zone of tensile stress. Introduce a local Cartesian reference frame $(x,y)$ for each strut such that $x$ is the distance along the strut and $y$ is the distance from the neutral section. The stress distribution $\sigma_1(x,y) = F/t + 12My/t^3$ is obtained from the bending moment along the strut $M(x) = M_1 + (M_2 - M_1)x/\ell$ and the axial force $F$. By setting $\sigma_1(x,y) = 0$, we locate the position of the neutral axis as a function of the distance $x$ along the beam, $y_{NA}(x) = -Ft^2/12M(x)$. The integral within expression (29) then reads

$$\int_V g^m(r/\ell,\theta,\bar{t})\frac{rdrd\theta}{V_0} = \left(\frac{\ell^2}{V_0}\right)\left(\frac{\bar{t}\sqrt{\ell}}{K_I}\right)^m \int_V \sigma_1^m(\xi,\theta,\bar{t})\xi d\xi d\theta \tag{30}$$

where $\xi = r/\ell$ is used as a dummy variable. This integral is calculated over a square region of side $2R$ centered at the crack tip (Fig. 8). As the size of the square region increases, the volume integral

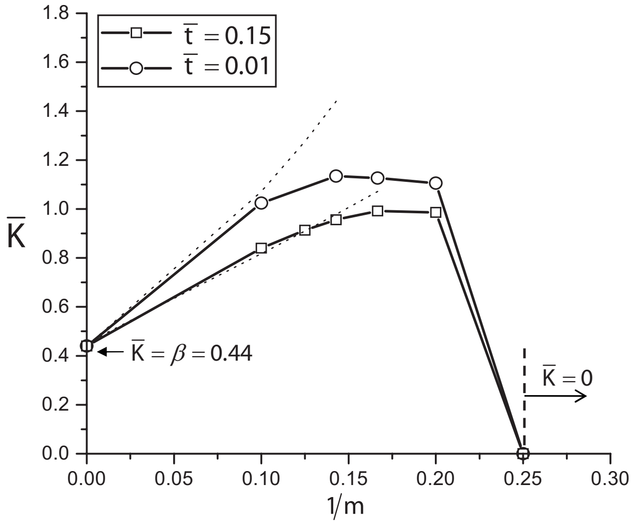


**Fig. 10 Dependence of $\bar{K}$ on the Weibull modulus. The dotted lines denote the analytical estimate of Eq. (33) for large *m*.**

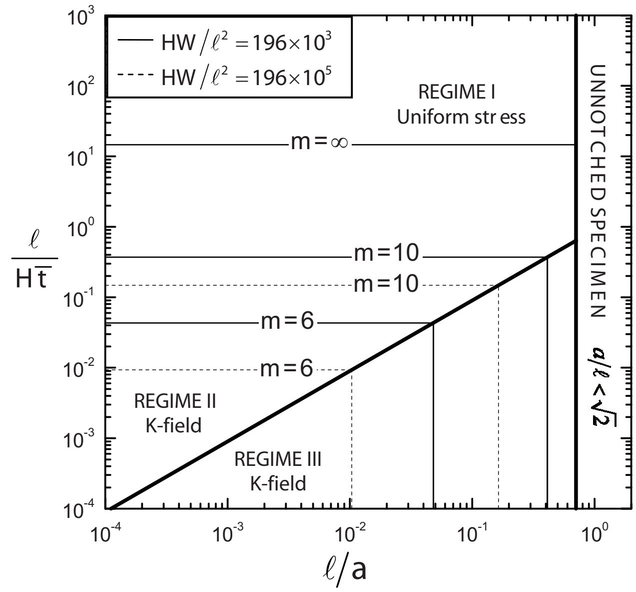


**Fig. 11 Fracture map for a honeycomb core sandwich panel where the statistical variability of the cell-wall strength is included**

in Eq. (30) converges to a constant value. The higher the Weibull modulus $m$, the faster the convergence is achieved.

The dependence of $\bar{K}\equiv(K_{IC})_{\text{mean}}/\sigma_0\bar{t}\sqrt{\ell}$ on Weibull modulus is plotted in Fig. 10 for the two values of cell-wall stubbiness, $\bar{t}=0.15$ and $\bar{t}=0.01$, with the arbitrary volume $V_0$ taken to be $V_0=\ell^2$. The plots display a peak value of fracture toughness for $m$ about equal to 6. A large Weibull modulus $m$ implies small variations in cell-wall strength, and deterministic fracture toughness, $\bar{K}=\beta=0.44$. However, at low $m$, the effect of a stochastic strength is significant. There exists a limit $m=4$ below which $\bar{K}$ drops to zero. A scaling argument can be used to explain this. Conventional linear elastic fracture mechanics suggests that the nondimensional function $g$ scales with distance $r$ from the crack tip as $g\propto r^{-1/2}$. Therefore, the integral within Eq. (29) has the following scaling:

$$\int_V g^m dV \propto \int_V r^{-m/2} r\,d\theta\,dr \propto \int_\delta^\infty r^{2-m/2}dr \approx \frac{2}{4-m}[r^{4-m/2}]_{r=\delta}^{r=\infty} \tag{31}$$

where the lower limit of integration $\delta$ is on the order of the cell size of the lattice $\ell$. Note that this integral has a finite value for $m>4$; however, for $m\leq 4$ the integral is unbounded at the outer limit and $\bar{K}$ equals zero. We conclude from Eq. (28) that the fracture toughness of the lattice tends to zero for $m\leq 4$. The physical interpretation is the following: The variability in strength is sufficiently great for $m\leq 4$ that struts remote from the crack tip fail and the effective "stressed volume" is unbounded.

*4.2.3 Analytical Estimate of the Mean Fracture Toughness.* For large values of Weibull modulus $m$, failure always occurs near the crack tip. An estimate for the mean fracture toughness is found by considering only the critical strut directly ahead of the crack tip (Fig. 2). Assume that this critical strut deforms as a built-in beam, as sketched in Fig. 3(*a*). Ignore the tensile stress caused by axial and shear forces so that only the tensile stress due to bending is taken into account. The survival probability is given in terms of the maximum local bending stress in the built-in beam $\sigma_A$ by [14]

$$P_s = \exp\left[-\frac{1}{2(m+1)^2}\left(\frac{V}{V_0}\right)\left(\frac{\sigma_A}{\sigma_0}\right)^m\right] \tag{32}$$

Here, the volume $V$ per unit depth is equal to $2\ell t$ since only two struts are critical: the one containing the fracture site A, as shown in Fig. 2, and its mirror image about the cracking plane. Numerical investigations [4] have revealed that the maximum local bending stress $\sigma_A$ in the beam reads $\sigma_A=K_I/0.44\bar{t}\sqrt{\ell}$. Substitution of this value into Eq. (32) provides

$$\bar{K}\equiv\frac{(K_{IC})_{\text{mean}}}{\sigma_0\bar{t}\sqrt{\ell}} = \Gamma\left(\frac{m+1}{m}\right)\left[0.44^m(1+m)^2\left(\frac{V_0}{\ell^2}\right)\frac{1}{\bar{t}}\right]^{1/m} \tag{33}$$

Equation (33) is plotted in Fig. 10 as a dotted line for the two values of $\bar{t}$ considered in the numerical calculation of the previous section. As expected, the estimate is valid only for large $m$. For example, for $m>10$, the error is less than 4%. However, the analytical estimate considerably deviates from the numerical calculation of $\bar{K}$ as the Weibull modulus is decreased.

**4.3 Implications of Weibull Statistics on the Fracture Map.** The variability in cell-wall strength leads to a variability in strength of the cracked sandwich panel in Regime I of the fracture map, recall Eq. (8). Likewise, the variability in fracture toughness leads to a variability in strength of the cracked sandwich panel, recall Eqs. (18) and (21) for Regimes II and III, respectively.

The implications of cell-wall strength variability on the fracture map are now examined. We make use of expressions (25) and (33) in order to derive analytical estimates for the boundaries between regimes.

First, consider the boundary between Regimes I and II. Upon equating the mean strength (25) in Regime I with the mean strength in Regime II, as specified by Eqs. (18) and (33), we obtain

$$\frac{\ell}{H\bar{t}} = \frac{2\sqrt{2}}{\beta^2}\left[\frac{1}{2(1+m)^2}\left(\frac{\ell^2}{2HW}\right)\right]^{2/m} \tag{34}$$

Second, the boundary between Regimes I and III is obtained via Eqs. (25), (21), and (33), giving

$$\frac{\ell}{a} = \frac{\pi}{\beta^2}\left[\frac{1}{2(1+m)^2}\left(\frac{\ell^2}{2HW}\right)\right]^{2/m} \tag{35}$$

Third, the boundary between Regimes II and III is obtained by equating the strengths as specified by Eqs. (18) and (21); Note that this boundary is insensitive to the value of $m$.

The effect $m$ on the boundaries of the fracture map is shown in Fig. 11. Boundaries are plotted for selected values of $m=10$ and

$m=6$ together with the deterministic result $m=\infty$. It is clear that as the Weibull modulus decreases the regimes of fracture toughness control shrink in favor of the strength-governed Regime I.

Boundaries are given in Fig. 11 for two values of $HW/\ell^2$. One choice corresponds to the geometry considered in the FE analysis of the present study such that $W/H=20$ and $H/\ell=70\sqrt{2}$, giving $HW/\ell^2=196\times10^3$. A second choice assumes a much larger structure such that $W/H=20$ and $H/\ell=700\sqrt{2}$, giving $HW/\ell^2=196\times10^5$. It is clear from Fig. 11 that for finite $m$ Regime I expands with increasing volume of panel, for a given cell size $\ell$.

Engineering ceramics have a wide range of $m$ value from 3 to 20 depending on the processing route. For example, cordierite in catalytic converters has approximately $m=6$ [6]. Thus, it is necessary to include statistical effects on the strength of the sandwich panel.

## 5 Concluding Remarks

In this study, it is shown that the fracture strength of a center-cracked sandwich panel made from a brittle diamond-celled honeycomb depends on the relative density of the lattice, the crack size, and the geometric dimensions of the panel. The FE method has been used to investigate the damage tolerance of the structure. A fracture map has been constructed with axes $(\ell/a, \ell/\bar{t}H)$ given by the sandwich geometry. Three regimes of behavior have been observed. Simple analytical models of each regime are able to capture the mechanical response of the sandwich panel.

Statistical variations in the cell-wall strength have been quantified by assuming that it follows a Weibull distribution. The effect of specimen geometry and Weibull modulus on the fracture map has been explored. As expected, a large sandwich panel is more likely to be strength controlled, for a given cell size of the honeycomb. It is also found that the domain of toughness-controlled fracture shrinks as the Weibull modulus $m$ is decreased. For $m \leq 4$, the fracture toughness of the honeycomb falls to zero and failure is strength governed.

The results presented above give the fracture toughness of the lattice $K_{IC}$ in terms of the tensile strength $\sigma_f$ of the cell-wall material. However, $\sigma_f$ derives from the fracture toughness $K_s$ of the cell wall and the intrinsic flaw size $c$ within the cell walls

$$\sigma_f \approx \frac{K_s}{\sqrt{\pi c}} \tag{36}$$

Substition of Eq. (36) into Eq. (1) gives

$$\frac{K_{IC}}{K_s} = 0.23\bar{t}\left(\frac{\ell}{c}\right)^{1/2} \tag{37}$$

This alternative presentation of the fracture toughness $K_{IC}$ suggests that improved processing techniques, which reduce $c$, will lead to an enhanced toughness of the lattice.

The current study is also of relevance to the fatigue strength of *metallic* lattices. Following Gibson and Ashby [2] and Huang and Lin [15], we argue that fatigue failure of the cracked lattice is due to the cyclic failure of the most heavily loaded strut. Now limit attention to the fatigue limit of the lattice. At infinite fatigue life, this critical strut is subjected to local stress of amplitude equal to the endurance limit $\sigma_e$ of the solid. The map shown in Fig. 4 can be reinterpreted as a fatigue fracture map for infinite life once we rewrite $\bar{\sigma}$ as amplitude of net-section fatigue loading normalized by $\sigma_e$. Also, the stress intensity range for fatigue crack growth in the metallic lattice $\Delta K_{\mathrm{th}}$ can be directly stated from Eq. (1) as

$$\Delta K_{\mathrm{th}} = 2\beta\sigma_e\bar{t}\sqrt{\ell} \tag{38}$$

The authors are unaware of any experiments in the literature, which support or refute Eq. (38). Formulas similar to Eq. (38) have been developed for open-cell metallic foams and polymeric foams, see Gibson and Ashby [2], Olurin et al. [16], and Burman and Zenkert [17]. These experimental and theoretical studies support the idea that the fatigue crack growth threshold $\Delta K_{\mathrm{th}}$ is dependent on the cyclic fatigue strength $\sigma_e$ of the cell wall and on the cell size $\ell$. The authors are unaware of any experimental studies, which can be used to validate the fracture and fatigue maps presented here. It is suggested that such validation is a topic for future study.

## Acknowledgment

The authors are grateful for the support provided by the EPSRC and by the European Community's Human Potential Programme HPRN-CT-2002-00198 (RTN-DEFINO).

## References

[1] Ashby, M. F., 1983, "The Mechanical Properties of Cellular Solids," Metall. Trans. A, **14A**, pp. 1755–1783.
[2] Gibson, L. J., and Ashby, M. F., 1999, *Cellular Solids: Structure and Properties*, 2nd ed., Pergamon, Oxford.
[3] Fleck, N. A., and Qiu, X., 2007, "The Damage Tolerance of Elastic-Brittle, Two Dimensional Isotropic Lattices," J. Mech. Phys. Solids, **55**(3), pp. 562–588.
[4] Romijn, N. E., and Fleck, N. A., 2007, "The Fracture Toughness of Planar Lattices: Imperfection Sensitivity," J. Mech. Phys. Solids, **55**(12), pp. 2538–2564.
[5] Quintana Alonso, I., and Fleck, N. A., 2007, "Damage Tolerance of an Elastic-Brittle Diamond-Celled Honeycomb," Scr. Mater., **56**(8), pp. 693–696.
[6] Huang, J. S., and Gibson, L. J., 1991, "Fracture Toughness of Brittle Honeycombs," Acta Metall. Mater., **39**(7), pp. 1617–1626.
[7] Huang, J. S., and Chou, C. Y., 1999, "Survival Probability for Brittle Honeycombs Under In-Plane Biaxial Loading," J. Mater. Sci., **34**(20), pp. 4945–4954.
[8] Zupan, M., Deshpande, V. S., and Fleck, N. A., 2004, "The Out-of-Plane Compressive Behaviour of Woven-Core Sandwich Plates," Eur. J. Mech. A/Solids, **23**(3), pp. 411–421.
[9] Tada, H., Paris, P. C., and Irwin, G. R., 1985, *The Stress Analysis of Cracks Handbook*, St. Louis, MO.
[10] Georgiadis, H. G., and Papadopoulos, G. A., 1988, "Cracked Orthotropic Strip With Clamped Boundaries," J. Appl. Math. Phys., **39**(4), pp. 573–578.
[11] Bowie, O. L., and Freese, C. E., 1972, "Central Crack in Plane Orthotropic Rectangular Sheet," Int. J. Fract. Mech., **8**(1), pp. 49–57.
[12] Savin, G. N., 1961, *Stress Concentration Around Holes*, Pergamon, Oxford.
[13] Sih, G. C., Paris, P. C., and Irwin, G. R., 1965, "On Cracks in Rectilinearly Anisotropic Bodies," Int. J. Fract. Mech., **1**(3), pp. 189–203.
[14] Jayatilaka, A. de S., 1979, *Fracture of Engineering Brittle Materials*, Applied Science, London.
[15] Huang, J. S., and Lin, J. Y., 1996, "Fatigue of Cellular Materials," Acta Mater., **44**(1), pp. 289–296.
[16] Olurin, O. B., McCullough, K. Y. G., Fleck, N. A., and Ashby, M. F., 2001, "Fatigue Crack Propagation in Aluminium Alloy Foams," Int. J. Fatigue, **23**, pp. 375–382.
[17] Burman, M., and Zenkert, D., 1997, "Fatigue of Foam Core Sandwich Beams," Int. J. Fatigue, **19**(7), pp. 551–578.